The Hydrogen Molecule in Strong Magnetic Fields: Optimizations of Anisotropic Gaussian Basis Sets

Atsushi Kubo†

Department of Chemistry, Graduate School of Science, Kyoto University, Kyoto 606-8502, Japan

Received: January 30, 2007

The anisotropic Gaussian basis sets were optimized for the H atom and the hydrogen molecule in strong magnetic fields of 0−1000 a.u. We used five-parameter fit functions to generate anisotropic Gaussian exponents of hydrogenic atomic orbitals. These functions provided errors of energy that were comparable to the independent optimization of all the exponents. The optimal exponents were used to calculate the Hartree−Fock energies of H_2 at arbitrary orientations, with respect to the magnetic field. Furthermore, the double-exponential transformation was applied to calculate highly anisotropic Coulomb integrals. Between magnetic field strengths of 1 a.u. and 100 a.u., a molecule in a triplet ground state continuously changed its stable orientation from the perpendicular geometry to the parallel geometry.

Introduction

Strong magnetic fields have been applied to investigate the electronic structures of conducting materials. For example, the de Haas van Alphen effect has been used to measure the Fermi surface of bulk metals.[1,2] The key element of the phenomenon is that the energy levels of electrons are quantized in the magnetic field. Furthermore, a set of degenerate levels moves across the Fermi surface, as a magnetic field increases. In other words, the magnetic field induces transitions between the highest occupied molecular orbital (HOMO) and the lowest unoccupied molecular orbital (LUMO). Because of the succesive transitions, the magnetization and the other properties oscillate in the period proportional to the inverse of field strength.

The same type of phenomenon occurs when electrons are confined in a ring-shaped material or a cylindrical material. This is usually referred to as the Aharonov−Bohm (AB) effect. In the AB effect, the quantization is due to the circular boundary condition. The transitions occur between two states that have different angular momentum values. The spin Zeeman interactions are usually ignored, compared to the orbital Zeeman interactions, because of the large area surrounded by the material. The period between successive transitions is determined from the flux quantization condition. The subsequent transition occurs when the flux penetrating the conducting ring increases by a quantum flux $\Phi_0 = h/e$ from the preceding transition field. The direction of the persistent current is reversed by these transitions.[3−5] The AB effect has been studied for superconducting rings,[6−8] mesoscopic metal rings,[9] and semiconductor quantum dots.[10,11] More recently, the intensive studies of this effect have been performed on carbon nanotubes.[12−17]

It is natural to extend such studies on bulk, mesoscopic, and nanosized materials to those of small molecular systems, where very accurate quantum mechanical calculations are possible.[18−20] However, there is an obstacle to this extension. To induce the level crossing in molecular systems, the required magnetic field strength is often close to 1 a.u. (i.e., 2.35×10^5 T). Electronic states in such strong fields have been studied by atomic physicists,[21,22] and later by astrophysicists,[23] who were interested in the materials near white dwarfs and neutron stars. According to these works, electronic clouds of atoms do not have the spherical symmetry any more. They contract in the plane perpendicular to a magnetic field due to the strong Lorentz force. Therefore, if molecular or atomic orbitals were expanded by the isotropic Slater or Gaussian functions, a great number of primitive orbitals with high angular momentum were required.[24,25] Intensive studies have been performed on the hydrogen atom to improve the accuracy of energies and wavefunctions. Recently, Kravchenko et al. developed a computational method that provides exact power series solutions of the hydrogenic Schrödinger equation in a magnetic field of arbitrary strength.[26−28] The binding energies of the ground state and several excited states were reported with an accuracy of 10^{-12} hartree for a field strength of 1×10^{-4}−4×10^3 a.u. Reviews,[29,30] books,[31,32] and conference papers[33] have been published on this subject.

For the molecular quantum chemical calculations in field free space, the Gaussian basis sets have long ago become a standard method.[34−37] In strong magnetic fields, various methods have been examined for the two different molecular systems, the H_2^+ ion[38,39] and the H_2 molecule.[40−43] For extremely strong fields ($>1 \times 10^8$ T), i.e., 420 a.u., Landau-type orbitals have been applied. H atoms were shown to form stable infinite chains in a field greater than 400 a.u.[44−46] For intermediate field strengths of 0−100 a.u., Schmelcher and Cederbaum introduced anisotropic Gaussian primitive orbitals to expand the molecular orbitals effectively.[47] They also multiplied the London's gauge factors to the Gaussian orbitals to form the gauge-invariant atomic orbitals (GIAOs).[48,49] Hereafter, we refer to the method as the anisotropic GIAO method.

Schmelcher and co-workers have been successful in applying this anisotropic GIAO method to molecular systems such as the H_2^+ ion[50−54] and the H_2 molecule[55,56] in a field range of 0−100 a.u. These works replaced the previous works, because of improved accuracy. For example, they determined the transition field strengths of H_2; the ground state changes from $^1\Sigma_g$ to $^3\Sigma_u$ at a magnetic field of 0.18 a.u. and becomes $^3\Pi_u$ at >12.3 a.u. However, they have investigated only the parallel

† Author to whom correspondence should be addressed. E-mail address: a.kubo@kuchem.kyoto-u.ac.jp.

10.1021/jp070809z CCC: $37.00
Published on Web 06/02/2007

geometry of the molecular axis, with respect to magnetic fields. In the preceding studies on the H_2^+ ion, they have presented two-dimensional potential energy surfaces as a function of bond length and orientation. The energy minima of some excited states appeared at the arbitrary angles in the range of 0°−90°. Therefore, it is also possible that the ground states of H_2 have potential minima other than those in the parallel geometry.

Schmelcher et al.,[57] as well as other researchers who tested the anisotropic GIAO method,[58] applied rather large basis sets. To extend the studies to larger molecules or atoms, we must know how to generate compact and efficient basis sets for a given error level. Moreover, to enable the studies on field-dependent properties of molecules, systematic methods must be known, rather than numerical tables of the basis sets at several field strengths. In this paper, we will reinvestigate the anisotropic GIAO method in these aspects. Furthermore, we apply the method to investigate the field dependence of the potential energy surface of the H_2 molecule.

Optimization of the Hydrogen Atomic Orbital

Before examining the molecular electronic structure, we must determine the basis sets that will be used to expand the molecular orbitals. In the absence of a magnetic field, those procedures to determine the most effective basis sets for a given accuracy have been documented in detail.[36,37] However, there seems to be less knowledge for the basis sets in strong magnetic fields. In this section, we will describe the method to optimize the hydrogen basis sets and subsequently present the results of optimizations. The procedures to evaluate the molecular integrals are given in the Appendix. As shown in Appendix A-4, the double-exponential transformation[59] was efficient to calculate numerically highly anisotropic Coulomb integrals.

According to the recipes of Schmelcher and co-workers, we can expand the hydrogen atomic wave function by the anisotropic Gaussian orbitals, χ_k^{m,ν_z}:

$$\Phi_{m,\nu_z}(x,y,z) = \sum_{k=1}^{N_g} c_k \chi_k^{m,\nu_z} \tag{1}$$

where N_g is the number of primitive Gaussian functions and χ_k^{m,ν_z} is given by

$$\chi_k^{m,\nu_z}(x,y,z) = N_{m,\nu_z}(\hat{\zeta}_k)\{x + i\,\mathrm{sgn}(m)y\}^{|m|} z^{\nu_z} \exp\{-\zeta_{\perp,k}(x^2 + y^2) - \zeta_{z,k}z^2\} \tag{2}$$

where m is the magnetic quantum number and ν_z is the z-parity. The normalization factor ($N_{m,\nu_z}(\hat{\zeta}_k)$) is given by

$$N_{m,\nu_z}(\hat{\zeta}_k) = \{\pi^{3/2}(2\zeta_{\perp,k})^{-(m+1)}(2\zeta_{z,k})^{-1/2(2\nu_z+1)} m!\, 2^{-\nu_z} \times (2\nu_z - 1)!!\}^{-1/2} \tag{3}$$

The expansion coefficients $\vec{c}^{\,\mathrm{T}} = [c_1 \cdots c_{N_g}]$ are obtained by solving the eigenvalue equation:

$$\sum_k \langle \chi_j^{m,\nu_z} * |\hat{H}| \chi_k^{m,\nu_z} \rangle c_k = \epsilon_{m,\nu_z} \sum_k \langle \chi_j^{m,\nu_z} * |\hat{S}| \chi_k^{m,\nu_z} \rangle c_k \tag{4}$$

where $\hat{H}$ is the one-electron Hamiltonian and $\hat{S}$ is the overlap matrix. $\chi_j^{m,\nu_z}*$ is the complex conjugate of χ_j^{m,ν_z}.

The ground-state energy within the (m,ν_z) manifold (ϵ_{m,ν_z}^1) was optimized with respect to the $2N_g$ parameter sets $\{\zeta_{\perp,k},\zeta_{z,k}\}$. The optimization procedure used the gradient of ϵ_{m,ν_z}^1, with respect to the exponents, which can be calculated by the following equation:

$$\nabla_{\vec{\zeta}} \epsilon_{m,\nu_z}^1 = \frac{\vec{c}^{\,\mathrm{T}} \cdot (\nabla_{\vec{\zeta}} \hat{H} - \epsilon_{m,\nu_z}^1 \nabla_{\vec{\zeta}} \hat{S}) \cdot \vec{c}}{\vec{c}^{\,\mathrm{T}} \cdot \hat{S} \cdot \vec{c}} \tag{5}$$

In the aforementioned equation, the gradient matrices $\nabla_{\vec{\zeta}}\hat{H}$ and $\nabla_{\vec{\zeta}}\hat{S}$ are obtained from the matrix elements of $\hat{H}$ and $\hat{S}$ for the higher polarization states, because the following relations are satisfied for the derivatives of basis sets:

$$\frac{\partial}{\partial \zeta_{\perp,k}} \chi_k^{m,\nu_z} = \left\{ \frac{m+1}{2\zeta_{\perp,k}} - (x^2 + y^2) \right\} \chi_k^{m,\nu_z} \tag{6}$$

$$\frac{\partial}{\partial \zeta_{z,k}} \chi_k^{m,\nu_z} = \left\{ \frac{2\nu_z + 1}{4\zeta_{z,k}} - z^2 \right\} \chi_k^{m,\nu_z} \tag{7}$$

The independent optimization of all the $2N_g$ parameters was possible, even for $N_g = 10$. However, the initial parameters must be set close to the final optimized values, otherwise, the optimization proceeds very slowly. Therefore, the initial sets must be obtained from a few parameter optimization by assuming suitable relations between $\{\zeta_{\perp,k},\zeta_{z,k}\}$. The variational calculations of the hydrogenic atom and the molecular ion H_2^+ often used the mixed Slater−Gaussian-type orbitals, which are expressed by[60−64]

$$\psi \approx \exp(-ar - b\rho^2)$$

The parameter b vanishes when the magnetic field strength B_0 is zero. It approaches a value of $^1/_4 B_0$ as B_0 increases. Because the Slater function can be expanded by Gaussian functions,[65] we can assume some relation between the perpendicular exponents and the z-exponents; $\zeta_{\perp,k} = \zeta_{\perp,k}(\zeta_{z,k},B_0)$. We will test the following two-step procedure to generate the exponents. At first, the parallel components of the exponents were generated by

$$\begin{aligned} \zeta_{z,k} &= \zeta_{z,1} \exp\{-(k-1)^\gamma \ln \beta\} \\ &= \zeta_{z,k_0} \exp\{\ln \beta[(k_0 - 1)^\gamma - (k-1)^\gamma]\} \end{aligned} \tag{8}$$

where

$$k_0 = \mathrm{int}\left(\frac{N_g}{2}\right) + 1 \tag{9}$$

The aforementioned equation reproduces the Huzinaga's 10 exponents of the H 1s orbital, when $\zeta_{z,1} = 1170.498$, $\beta = 6.7$, and $\gamma = 0.785$.[35] We examined two functions that generated the perpendicular components $\zeta_{\perp,k}$ from $\zeta_{\perp,k}$ and B_0. The first function was given by

$$\zeta_{\perp,k} = \left\{ \zeta_{z,k}^{\ \delta} + \left(\frac{1}{4} B_0\right)^\delta \right\}^{1/\delta} \tag{10}$$

where δ was fixed toa value of 2.35. The three parameters (ζ_{z,k_0}, β, and γ) in eq 8 were optimized. The second function was given by

$$\zeta_{\perp,k} = B_0 \sqrt{\frac{1}{16} + \frac{\eta(\zeta_{z,k}/B_0) + (\zeta_{z,k}/B_0)^2}{1 + \xi(B_0/\zeta_{z,k})^2}} \tag{11}$$

where η and ξ were variables. The total five parameters were optimized under the restriction $\xi \geq 0$.

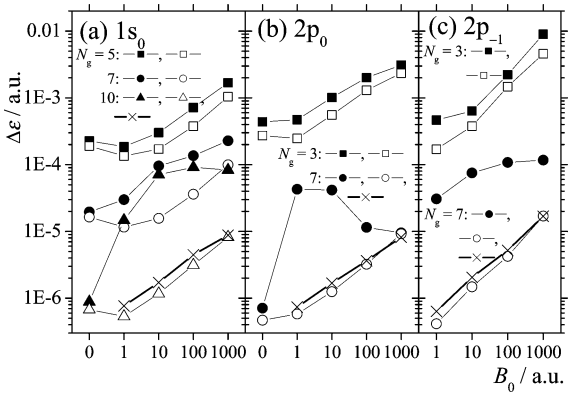

Figure 1. Errors in the orbital energy of an atomic hydrogen calculated with the anisotropic Gaussian basis sets. The errors were measured from the exact values of ref 27. The closed characters were obtained by the optimization using eqs 8−10. These sets of exponents were used as the initial parameters in the independent optimization of all the exponents. The results are shown by the open characters. The different characters are used to distinguish the numbers of Gaussian orbitals N_g. The crosses (×) correspond to the results of the optimizations using eqs 8, 9, and 11. This optimization was performed only for the largest values of N_g. The notations $1s_0$, $2p_0$, and $2p_{-1}$ refer to the lowest-energy levels with the symmetry $(m,\nu_z) = (0,0)$, $(0,1)$, and $(-1,0)$, respectively.

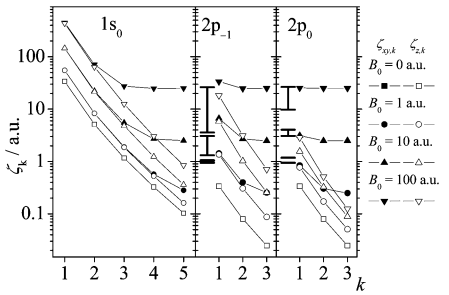

Figure 2. Optimal exponents of the 5s1p and the 5s3p basis sets. The 5s orbitals and the 3p orbitals for the different polarizations, $2p_{-1}$ and $2p_0$, were determined by the energy optimazations of a hydrogen (H) atom. All the exponents were varied independently. The perpendicular components $\zeta_{\perp,k} = \zeta_{xy,k}$ are represented by the closed characters, whereas the z-components, $\zeta_{z,k}$, are represented by the open characters. The exponents of the 1p orbitals are represented by the two connected bars. The upper holizontal bars represent the values of $\zeta_{\perp,1}$, whereas the lower bars represent those of $\zeta_{z,1}$. The exponents increase monotonically, as the field strength increases. These values were obtained from the energy optimizations of the singlet state of a H_2 molecule.

The results of the optimizations are summarized in Figure 1. The error in energy was calculated by using the exact energies reported by Kravchenko et al.[27] The errors of the optimization based on eqs 8−10 are much larger than those of the independent optimization, when N_g is the largest. However, eqs 8, 9, and 11 provided the comparable values to those of the independent optimization.

Kravchenko and Liberman proposed a different scheme to generate the $1s_0$ hydrogen basis sets in strong magnetic fields.[57] They used the even-tempered exponents,[66,67] which corresponded to $\gamma = 1$ in eq 8. Furthermore, they used the multiple sets $\{\zeta^j_{\perp,k},\zeta_{z,k}\}$, where the total number of j was 1−5. They obtained errors between 10^{-9} hartree and 10^{-6} hartree for the fields of 1−1000 a.u., using 70 Gaussian functions. Forty Gaussian functions were applied to obtain accuracy that is comparable to our best results. Thus, our results are a factor of 4 more economical than these results.

Some of the optimal exponents are plotted in Figure 2. These were obtained by the independent optimization of all the exponents. The optimal parameters based on eqs 8, 9, 11 are listed in Table 1. In Figure 2, the curves of the z-components $\zeta_{z,k}$ shift upward, as the magnetic field increases. The magnitudes of shifts are different for the three types of polarization. The $2p_{-1}$ polarization shows the largest shifts. The perpendicular components $\zeta_{xy,k} = \zeta_{\perp,k}$ are close to $\zeta_{z,k}$, when $\zeta_{z,k} \gg {}^1/_4B_0$. They are saturated at the levels of ${}^1/_4B_0$, when $\zeta_{z,k} \ll {}^1/_4B_0$. This means that electrons are confined within the region of $\sqrt{x^2+y^2} \leq 2/\sqrt{B_0}$.

TABLE 1: Best-Fit Parameters of Hydrogen Atomic Orbitals, According to Eqs 8, 9, and 11

B_0 (a.u.)	γ	$\zeta_{z,k0}$	β	η	ξ
		$1s_0$, $N_g = 10$			
1	0.75	3.95875	7.12537	0.0424609	0.0291636
10	0.71	10.4565	10.5976	0.120107	0.0388161
100	0.71	31.5400	12.0437	0.162815	0.0371274
1000	0.71	54.2199	11.1100	0.184319	0.0341019
		$2p_0$, $N_g = 7$			
1	0.84	0.388684	3.65292	0.125198	0.0282317
10	0.84	0.753819	3.93842	0.139638	0.0141082
100	0.84	1.203698	4.28456	0.132807	0.00686369
1000	0.84	1.600656	4.60689	0.214121	0.00551230
		$2p_{-1}$, $N_g = 7$			
1	0.78	0.832207	5.05702	0.136032	0.0390614
10	0.81	3.00447	5.01371	0.241611	0.0440947
100	0.82	8.87282	5.16754	0.262666	0.0351179
1000	0.86	25.3203	4.73697	0.280796	0.0305946

The Hydrogen Molecule

In the first part of this section, we will examine the selection of basis functions, especially, the p-type polarization functions for the Hartree−Fock (HF) calculations of H_2 in strong magnetic fields. Next, we will use those basis functions to calculate the electronic energies and the wavefunctions, as a function of the magnetic field strength and the molecular geometry.

The hydrogen p-type orbitals are usually added to represent the distortion of the s-type atomic orbitals by the zero-field molecular orbital calculations. They are called the polarization functions.[68] The exponents of the polarization functions are usually determined to minimize the total molecular electronic energy. The exponents obtained by this procedure can be very different from those of the atomic 2p orbitals. For example, the 6-311G** basis set by Pople contains a hydrogen p-type polarization function with an exponent of 0.75; this value is comparable to the middle exponent of the five s-type functions.[69] On the other hand, the procedure is inappropriate for the triplet state, especially for the $^3\Pi_u$ state. The HOMO of this state consists mainly of the $2p_{-1}$ orbital. Therefore, it would be better to use the atomic 2p orbitals instead of optimizing a single set of p-functions.

Here, we will test the two types of basis sets. In both basis sets, we used the five Gaussian functions obtained via the energy optimization of the atomic $1s_0$ orbital. These were split to the inner, the intermediate, and the outer orbtals, which contained 3, 1, and 1 primitive Gaussian functions, respectively. In the first method, we added a single set of isotropic or anisotropic p-type Gaussian functions to the s-type set, and optimized their exponents and the bond length. The exponents of the p_z orbital were assumed to be different from those of the p_x and the p_y orbitals. The former exponents were determined by the calculations in the parallel geometry, whereas the latter were determined by those in the perpendicular geometry.

In the second method, we added the three sets of $2p_0$ exponents and the three sets of $2p_{-1}$ exponents obtained in the previous section without contractions. The former sets were used

TABLE 2: Total Energies and Equilibrium Bond Lengths of the Singlet States of H_2 versus Applied Magnetic Fields Obtained by Various Basis Sets[a]

	this work (HF)										
	basis set 5s1p (iso. p)[b]			basis set 5s1p (aniso. p)[c]				basis set 5s3p[d]		Detmer et al.[55] (CI)	
B_0 (a.u.)	ϵ (a.u.)	ζ_{2p}^{iso}	R_{HH} (a.u.)	ϵ (a.u.)	$\zeta_{2p,\perp}$	$\zeta_{2p,z}$	R_{HH} (a.u.)	ϵ (a.u.)	R_{HH} (a.u.)	ϵ (a.u.)	R_{HH} (a.u.)
						$\overrightarrow{HH} // \vec{B}_0$					
0	−1.1326	0.95	1.39					−1.1306	1.39	−1.173436	1.40
1	−0.8465	1.2	1.22	−0.8465	1.19	1.18	1.22	−0.8464	1.22	−0.890336	1.24
10	5.9532	3.7	0.69	5.9532	4.05	3.08	0.69	5.9535	0.69	5.889023	0.70
100	90.6370	21.0	0.33	90.6360	26.6	9.8	0.33	90.6388	0.33	90.506974	0.334
						$\overrightarrow{HH} \perp \vec{B}_0$					
1	−0.8159	1.06	1.15	−0.8159	1.06	1.03	1.16	−0.8172	1.16		
10	6.3332	3.0	0.56	6.3280	3.07	1.32	0.56	6.3234	0.56		
100	92.7329	25.0	0.225	92.6533	26.1	3.6	0.229	92.6362	0.23		

[a] The five optimal Gaussian functions of the $1s_0$ atomic orbital were used with the 3−1−1 contraction. [b] Single isotropic *p*-type Gaussians were added to the aforementioned 5s orbitals, and the exponent was optimized by minimizing the total molecular electronic energy. The optimal exponents are also listed. [c] Single anisotropic Gaussians were added to the aforementioned 5s orbitals, and the exponent was optimized by minimizing the total molecular electronic energy. The optimal exponents are also listed. [d] The three optimal Gaussian functions of the $2p_0$ and $2p_{-1}$ atomic orbitals were added to the 5s orbitals without contraction.

for the p_z orbitals, whereas the latter sets were used for both the p_x and p_y orbitals. Only the bond length was optimized in the second method. Hereafter, these two basis sets are referred to as 5s1p and 5s3p. Through this paper, we applied only the HF method to calculate the electronic energies. The wavefunctions obtained by this method are easily visualized. We describe the details of the algorithms to evaluate the molecular integrals in Appendices A-1−A-4.

The results of the optimizations for the singlet states are shown in Table 2. We also present the results of the configuration interaction (CI) calculations by Detmer et al. for comparison.[55] The energies of the 5s1p basis sets are always lower than those of the 5s3p basis sets, by $0.1-2.8 \times 10^{-3}$ a.u., when the magnetic field is parallel to the internuclear vector. However, this order is reversed for the perpendicular geometry. The energies of the 5s3p basis sets are lower than those of the 5s1p basis sets by $1.3-17.1 \times 10^{-3}$ a.u. The optimal exponents of the 5s1p basis are plotted in Figure 2 with bars. The upper horizontal bars correspond to $\zeta_{\perp,k}$, whereas the lower bars correspond to $\zeta_{z,k}$. The exponents are almost isotropic at $B_0 = 1$ a.u.; however, they becomes anisotropic for $B_0 \geq 10$ a.u. For the $2p_{-1}$ type polarization, the optimal exponents of the 5s1p sets are within the ranges of the atomic 3p exponents. However, for the $2p_0$-type polarization, the optimal values of $\zeta_{z,k}$ are always larger than those of the 3p exponents. The differences are noticeable for the field strengths of $B_0 \approx 0$ a.u. and $B_0 \geq 100$ a.u. The 5s3p set can be applied for the singlet state if a single set of p_z exponents is added.

The electronic energies of the singlet state were always the lowest when the molecule was parallel to the magnetic field. For confirmation, we have calculated the potential energy surface (PES), as a function of the interproton distance, and the rotational angle of the molecule, with respect to a magnetic field. We used the 5s3p basis set. The results are shown in Figure 3. This behavior of the preferred orientation is attributable to the diamagnetic nature of the singlet orbital, because the diamagnetic energy $^1/_8 B_0^2(x^2 + y^2)$ has a minimum in the parallel orientation. Because of the anisotropic shape of the $1s_0$ orbitals, the equilibrium bond length is much shorter in the perpendicular orientation than that of the parallel orientation. Therefore, the internuclear Coulomb repulsion also destabilizes the perpendicular orientation.

We repeated the same procedures for the triplet states, and the results are listed in Table 3. We also present the results of

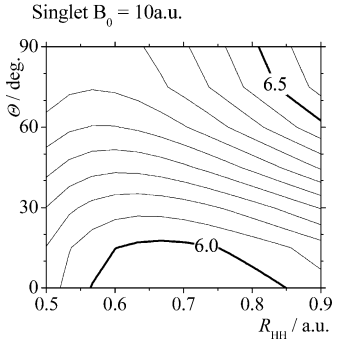

Figure 3. Total energy contour of the singlet H_2 system at $B_0 = 10$ a.u., plotted against the molecular geometries (R_{HH}, Θ).

the CI calculations by Detmer and co-workers.[55,56] For the triplet states, the 5s1p basis set was inappropriate in the field range ($B_0 \geq 10$ a.u.). This basis set always gave energies larger than those calculated with the 5s3p basis set. For the parallel orientation and $B_0 \leq 1$ a.u., both the basis sets provided almost the same energies, because the wavefunction was very close to those of two non-interacting atomic hydrogens in the $1s_0$ state. An interesting finding here was that the perpendicular orientation was the most stable at $B_0 = 1$ a.u., whereas the parallel orientation became the most stable at $B_0 = 100$ a.u. The molecule must change orientation between these two field strengths. For confirmation, we calculated the two-dimensional PESs at the three field strengths (1, 10, and 100 a.u.) and plotted them in Figure 4. At a field of 1 a.u., the potential minimum was located at (R_{HH}, Θ) = (2.8 a.u., 90°). The minimum moved to (R_{HH}, Θ) = (1.0 a.u., 37°) at $B_0 = 10$ a.u. and then to (0.38 a.u., 0°) at the largest field of $B_0 = 100$ a.u. The H_2 molecule changed the orientation continuously between 1 a.u. and 100 a.u. In Figure 4c, the PES shows a cusp at (R_{HH}, Θ) = (0.85 a.u., 0°). The present results agree with those of Zaucer and Azman,[40] who showed that the perpendicular orientation is more stable than the parallel one at $B_0 = 1$ a.u. Liberman and Peetrov reported the results which resemble but differ from the present calculations.[42] These authors performed variational calculations at the two field strengths of $B_0 = 50$ a.u. and 100 a.u. However, they ignored the fact that the two triplet states, $^3\Sigma_u$ and $^3\Pi_u$ could mix with each other for the general orientations of the H_2 molecule.

Naturally, the following question arises: How does the electron cloud deform during this continuous change of the

TABLE 3: Total Energies and Equilibrium Bond Lengths of the Triplet States of H_2 versus Applied Magnetic Field

	this work (HF)						
	basis set 5s1p (iso. p)[a]			basis set 5s3p[a]		Detmer and co-workers[55,56] (CI)	
B_0 (a.u.)	ϵ (a.u.)	ζ_{2p}^{iso}	R_{HH} (a.u.)	ϵ (a.u.)	R_{HH} (a.u.)	ϵ (a.u.)	R_{HH} (a.u.)
				$\overrightarrow{HH} // \vec{B}_0$			
0	−0.9995	0.012	7.6	−0.9995	7.6	−1.0000173	7.9
1	−1.6619	0.22	6.8	−1.6619	6.8	−1.6623090	7.5
10	No min.[b]			−3.4464	0.82	−3.466244	0.82
100	No min.[b]			−8.1794	0.38	−8.236318	0.38
				$\overrightarrow{HH} \perp \vec{B}_0$			
1	−1.66398	0.54	2.7	−1.66413	2.7		
10	No min.[b]			−3.4987 [−3.5504, $\Theta = 37°$][c]	0.91 [1.00]		
100	No min.[b]			No min.			

[a] The notations of 5s1p and 5s3p are the same as Table 2. [b] No potential minimum was obtained; the total energy was much larger than that obtained by the 5s3p set. [c] The potential minimum is located at (R_{HH}, Θ) = (1.00 a.u., 37°).

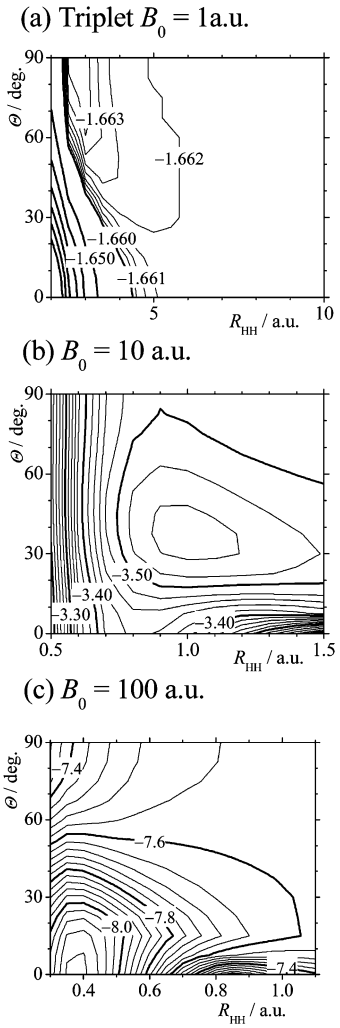

Figure 4. Total energy contours of the triplet H_2 system at the three magnetic field strengths, B_0 = 1, 10, and 100 a.u., plotted against the molecular geometries (R_{HH}, Θ).

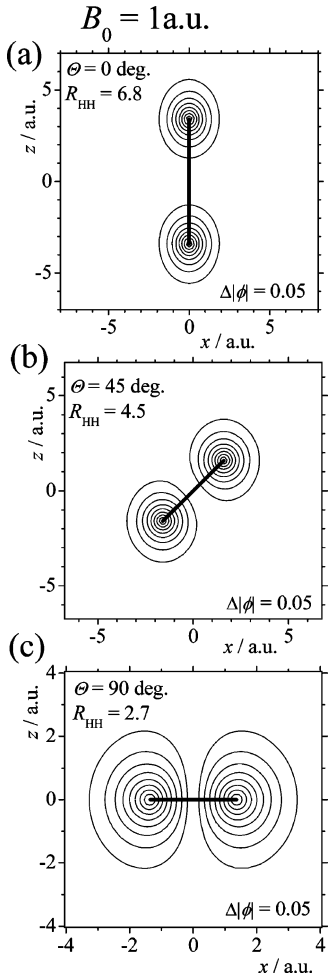

Figure 5. Contour maps of the HOMO wavefunction for the triplet H_2 system. A magnetic field of B_0 = 1 a.u. is applied along the *z*-axis. The amplitudes in the plane containing the two protons are plotted. The bond direction is shown by a thick line, the interproton distance R_{HH} is shown by the atomic unit, and $\Delta|\phi|$ is the separation between the contour lines.

molecular orientation, as the magnetic field increases? We have calculated the amplitude and the phase of the wavefunction on planes bisecting the molecule. For a H_2 molecule in its general orientation, with respect to the magnetic field, the rotational symmetry is lost and there is only the inversion symmetry with respect to the molecular center. The lowest orbital of the triplet ground state is related to the gerade symmetry and does not have any nodes or nodal lines. On the other hand, the HOMO belongs to the ungerade symmetry and has a single node or a single nodal line passing through the center of the molecule. The phase of the HOMO changes 2π through the path rounding the nodal line. In Figures 5−7, we plotted the amplitudes of the HOMO at three different field strengths and for different molecular geometries.

At B_0 = 1 a.u. and at $\Theta = 0°$, the HOMO is the $1\sigma_u$ orbital, as shown in Figure 5a. The amplitude of the HOMO has two maxima, which are completely separated by a nodal plane. In

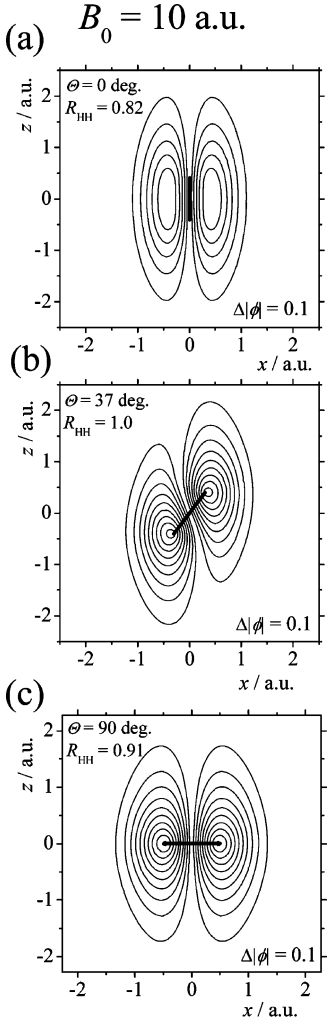

Figure 6. Contour maps of the HOMO wavefunction for the triplet H_2 system at a magnetic field strength of $B_0 = 10$ a.u. The amplitudes in the plane containing the two protons are plotted. The bond direction is shown by a thick line, the interproton distance R_{HH} is shown by the atomic unit, and $\Delta|\phi|$ is the separation between the contour lines.

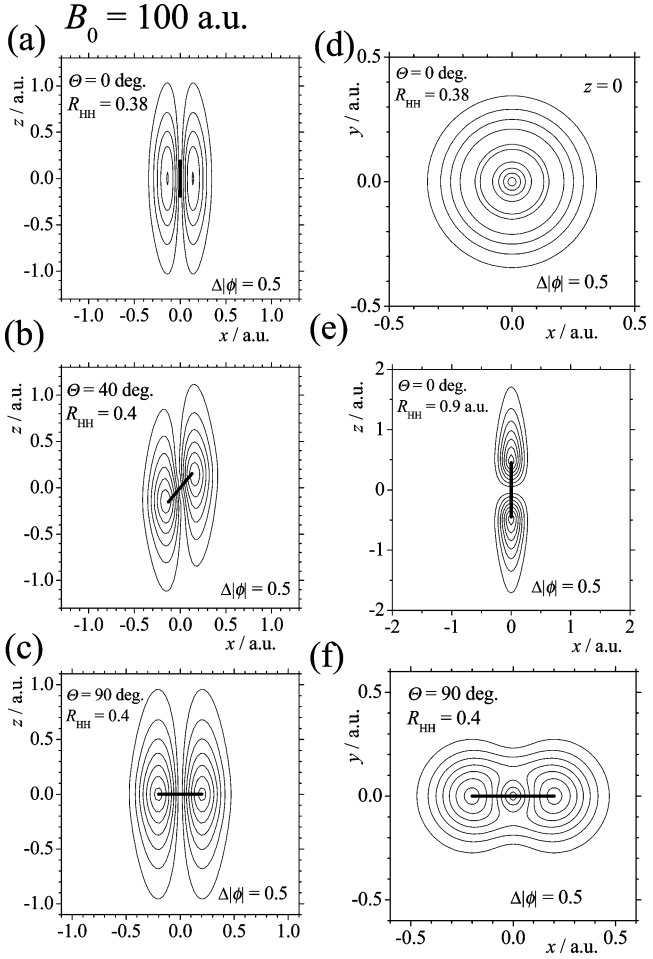

Figure 7. Contour maps of the HOMO wavefunction for the triplet H_2 system at a magnetic field strength of $B_0 = 100$ a.u. The amplitudes in the *xz*-plane containing the two protons are plotted in panels a, b, c, and e. The bond direction is shown by a thick line, the interproton distance R_{HH} is shown by the atomic unit, and $\Delta|\phi|$ is the separation between the contour lines. Panels d and f are the contour maps in the *xy*-plane containing the molecular center. The former was calculated for the molecular geometries identical to that of panel a, and the latter corresponds to panel c. Panel e was calculated for the orientation $\Theta = 0°$ and at an interproton distance slightly longer than the $^3\Pi_u - ^3\Sigma_u$ crossing point.

Figure 5c ($\Theta = 90°$), the nodal plane changes to a nodal line, and there is a finite electron density in the *xy*-plane. (See also Figure 7f for the plot in the *xy*-plane at the larger field of $B_0 = 100$ a.u.) Because of this continuous distribution of the electron density, the HOMO of Figure 5c has a little bonding character. Therefore, the perpendicular orientation becomes more stable than the parallel orientation at $B_0 = 1$ a.u.

At $B_0 = 10$ a.u. and $\Theta = 0°$, the HOMO changes to the $1\pi_u$ orbital, as shown in Figure 6a. When the molecule rotates to the orientations shown in Figures 6b and 6c, the orientation of the nodal line stays nearly parallel to the static magnetic field. At the potential minimum shown in Figure 6b, the HOMO is a distorted donut, which can be generated by mixing the $1\sigma_u$ and the $1\pi_u$ orbitals. The distinction between these two orbitals exists only with the parallel geometry of $\Theta = 0°$. For the general orientations, the HOMO changes continuously as a function of Θ and R_{HH}. When the interproton distance R_{HH} is varied on the line $\Theta = 0°$, a cusp appeared at $R_{HH} \approx 0.85$ in Figure 4c. We calculated the amplitude of the HOMO at $R_{HH} = 0.9$ and plotted it in Figure 7e. This figure does not compare with Figure 7a. The symmetry of the HOMO changed discontinuously from $1\pi_u$ to $1\sigma_u$ when R_{HH} increases across the cusp. Therefore, the cusp in Figure 4c is attributable to a conical intersection point between two energy levels belonging to the ungerade symmetry. Wille showed incompletely the existence of the conical intersections of a H_2^+ molecular ion in the magnetic field of 1 a.u.[39] Kappes and Schmelcher reported more-complete studies on the conical intersections of the same system.[51−54]

Appendix A-1. The Anisotropic GIAO Method

An Gaussian gauge-invariant atomic orbital (GIAO) centered at $\vec{C}$ with anisotropic exponents $\hat{\zeta}_c$ is given as

$$\vec{c}_C = \prod_{i=x,y,z} r_{i,C}^{\,c_i} \exp(-\vec{r}_C^{\,T} \cdot \hat{\zeta}_c \cdot \vec{r}_C - i\vec{A}_C \cdot \vec{r}_C) \qquad \text{(A1)}$$

where $\vec{r}_C = \vec{r} - \vec{C}$, and $\vec{c}$ is an integer vector, the sum of which is the angular momentum. $\vec{A}_C$ is the vector potential at $\vec{C}$:

$$\vec{A}_C = \frac{1}{2}\vec{B}_0 \times \vec{C} = \frac{1}{2}B_0\vec{e}_z \times \vec{C} \qquad \text{(A2)}$$

We choose the *z*-axis along the static magnetic field $\vec{B}_0$. With these coordinates, the exponent matrix $\hat{\zeta}_c$ is assumed to be diagonal:

$$\hat{\zeta}_c = \begin{bmatrix} \zeta_{c,\perp} & 0 & 0 \\ 0 & \zeta_{c,\perp} & 0 \\ 0 & 0 & \zeta_{c,z} \end{bmatrix} \tag{A3}$$

Schmelcher and Cederbaum proposed a unique method to generate the molecular integrals of the higher angular functions from those between the 1s Gaussian functions.[47] They introduce a new parameter $\vec{J}$ and multiplied the exponential function by the pair of the s-type primitive GIAO orbitals:

$$\{\vec{0}_C{}^*\vec{0}_D\}_{\vec{J}} = \vec{0}_C{}^*\vec{0}_D \exp(\vec{J}^T\cdot\vec{r}) \tag{A4}$$

The atomic orbitals with higher angular momentum were obtained by the differentiations with respect to the components of $\vec{J}$:

$$\vec{c}_C{}^*\vec{d}_D = \left[\prod_{i=x,y,z}\left(\frac{\partial}{\partial J_i} - C_i\right)^{c_i}\left(\frac{\partial}{\partial J_i} - D_i\right)^{d_i}\{\vec{0}_C{}^*\vec{0}_D\}_{\vec{J}}\right]_{\vec{J}=0} \tag{A5}$$

This algorithm is simpler than those that apply the differentiations, with respect to nuclear coordinates.[70−73] We also refer the reader to the recent paper by Ishida on isotropic GIAO integrals.[74]

The basic integrals were obtained in the same way as that done by Boys[34] and also by Singer.[75] The important modification from the ordinary molecular integrals is that the positional vector $\vec{P}$ is replaced by the complex vector $\vec{P}''$, which is given by the following equation:[47]

$$\vec{P}'' = \hat{\zeta}_{ab}{}^{-1}(\hat{\zeta}_a\vec{A} + \hat{\zeta}_b\vec{B}) + \frac{i}{2}\hat{\zeta}_{ab}{}^{-1}\vec{A}_{AB} + \frac{1}{2}\hat{\zeta}_{ab}{}^{-1}\vec{J} \tag{A6}$$

$$\hat{\zeta}_{ab} = \hat{\zeta}_a + \hat{\zeta}_b \tag{A7}$$

$$\vec{A}_{AB} = \vec{A}_A - \vec{A}_B \tag{A8}$$

The basic overlap integrals are calculated to be

$$(\vec{0}_A{}^*\vec{0}_B)_{\vec{J}} = \pi^{3/2}(\zeta_{ab,\perp}{}^2\zeta_{ab,z})^{-1/2}K_{AB}(\vec{P}'') \tag{A9}$$

where

$$K_{AB}(\vec{P}'') = \exp(\vec{P}''{}^T\hat{\zeta}_{ab}\vec{P}'' - \vec{A}^T\hat{\zeta}_a\vec{A} - \vec{B}^T\hat{\zeta}_b\vec{B}) \tag{A10}$$

The normalization constant is given by the following equation:

$$N_{\vec{a}} = \left(\frac{2}{\pi}\right)^{3/4}\prod_{i=x,y,z}\frac{\zeta_{a,i}{}^{1/4}(4\zeta_{a,i})^{a_i/2}}{\{(2a_i-1)!!\}^{1/2}} \tag{A11}$$

The basic electron nucleus attraction integrals are given by the following equations:

$$(\vec{0}_A{}^*r_C{}^{-1}\vec{0}_B)_{\vec{J}} \equiv 2\pi^{-1/2}\int_0^\infty du(\vec{0}_A{}^*\exp(-u^2r_C{}^2 + \vec{J}\cdot\vec{r})\vec{0}_B)$$
$$= 2\pi K_{AB}(\vec{P}'')I(\hat{\zeta}_{ab}, \overrightarrow{P''C})^{(\vec{0})} \tag{A12}$$

We will rewrite the aforementioned integral with the new variable t, which is given by the following equation:

$$I(\hat{\zeta}, \overrightarrow{P''C})^{(\vec{0})} = \int_0^\infty \frac{du}{(u^2+\zeta_\perp)(u^2+\zeta_z)^{1/2}} \times \exp\left\{-\frac{u^2\zeta_\perp\overline{P''C_\perp}^2}{u^2+\zeta_\perp} - \frac{u^2\zeta_z\overline{P''C_z}^2}{u^2+\zeta_z}\right\} \tag{A13}$$

$$t^2 = \frac{u^2}{u^2+\zeta_z} \tag{A14}$$

Equation A13 becomes

$$I(\hat{\zeta}, \overrightarrow{P''C})^{(\vec{0})} = \int_0^1 dt\,\frac{\zeta_\perp{}^{-1}}{1-t^2(\zeta_\perp-\zeta_z)/\zeta_\perp} \times \exp\left\{-\zeta_z\overline{P''C_\perp}^2\frac{t^2}{1-t^2(\zeta_\perp-\zeta_z)/\zeta_\perp} - \zeta_z\overline{P''C_z}^2t^2\right\} \tag{A15}$$

When $\zeta_\perp = \zeta_z$, the aforementioned integral reduces to the zeroth-order incomplete gamma function, F_0:

$$\lim_{\zeta_\perp,\zeta_z\to\zeta_{iso}}\zeta_\perp I(\hat{\zeta}, \overrightarrow{P''C})^{(\vec{0})} = \int_0^1 dt\exp(-\zeta_{iso}\overline{P''C}^2t^2) = F_0(\zeta_{iso}\overline{P''C}^2) \tag{A16}$$

The basic electron repulsion integrals (ERIs) are given by the following equation:

$$(\vec{0}_A{}^*\vec{0}_B r_{12}{}^{-1}\vec{0}_C{}^*\vec{0}_D)_{\vec{J}1,\vec{J}2} = 2\pi^{-1/2}\int_0^\infty du(\vec{0}_A{}^*\vec{0}_B \times \exp(-u^2r_{12}{}^2 + \vec{J}_1\cdot\vec{r}_1 + \vec{J}_2\cdot\vec{r}_2)\vec{0}_C{}^*\vec{0}_D) \tag{A17}$$

Here, two vectors $\vec{J}_1$ and $\vec{J}_2$ are introduced for the two electronic coordinates, $\vec{r}_1$ and $\vec{r}_2$, respectively. The final results reduce to the following form:

$$(\vec{0}_A{}^*\vec{0}_B r_{12}{}^{-1}\vec{0}_C{}^*\vec{0}_D)_{\vec{J}1,\vec{J}2} = 2\pi^{5/2}K_{AB}(\vec{P}'')K_{CD}(\vec{Q}'') \times \prod_{k=x,y,z}(\zeta_{ab,k}+\zeta_{cd,k})^{-1/2}I(\hat{\rho}, \overrightarrow{P''Q''})^{(\vec{0})} \tag{A18}$$

where $\vec{Q}''$ is the complex vector analogous to $\vec{P}''$, but for atoms C and D. The three components of the tensor $\hat{\rho}$ are given by the following equation:

$$\rho_k = \frac{\zeta_{k,ab}\zeta_{k,cd}}{\zeta_{k,ab}+\zeta_{k,cd}} \tag{A19}$$

The molecular integrals between the s-type orbitals are obtained from the aforementioned formulas, when $\vec{J}_i$ are set to the null value.

Appendix A-2. The Recurrence Relations between Electron Repulsion Integrals (ERIs)

To derive the recurrence relations between the ERIs,[73] we need only the following two relations for the differentiations, with respect to $\vec{J}_i$:

$$\frac{\partial}{\partial J_{k,1}}K_{AB}(\vec{P}'') = P_k''K_{AB}(\vec{P}'') \tag{A20}$$

$$\left(\frac{\partial}{\partial J_{k,1}}\right)I(\hat{\rho}, \overrightarrow{P''Q''})^{(\vec{n})} = -\zeta_{k,ab}{}^{-1}\rho_kP''Q_k''I(\hat{\rho}, \overrightarrow{P''Q''})^{(\vec{n}+\vec{1}_k)} \tag{A21}$$

TABLE 4: Comparisons of the Two Integration Methods: The Gauss−Legendre Quadrature Method (GL) and the Double-Exponential Formula (DE)

N_{point}	$I^{(\vec{0})}(\hat{\xi}, \overrightarrow{P'C_1})_{\text{GL}}{}^{a,b}$	$I^{(\vec{0})}(\hat{\xi}, \overrightarrow{P'C_1})_{\text{DE}}$	$I^{(\vec{0})}(\hat{\xi}, \overrightarrow{P'C_2})_{\text{GL}}{}^{a,c}$	$I^{(\vec{0})}(\hat{\xi}, \overrightarrow{P'C_2})_{\text{DE}}$
10	0.0118636102	0.0126819596	−0.0344932507	347.6521742820
14	0.0123507237	0.0126785910	0.4915735505	153.0265189884
19	0.0125756000	0.0126784402	−3.6922388008	316.9291153394
26	0.0126586630	0.0126784426	25.6166742405	257.1203955984
36	0.0126766118	0.0126784426	−113.0154738400	262.7458865742
50	0.0126783783	0.0126784426	−0.5707574670	262.8377134995
70	0.0126784420	0.0126784426	386.5494234809	262.8378762291
98	0.0126784426	0.0126784426	283.0116945927	262.8378762387
138	0.0126784426	0.0126784426	262.2019804186	262.8378762387
195	0.0126784426	0.0126784426	262.8385683866	262.8378762387
275	0.0126784426	0.0126784426	262.8378761198	262.8378762387
388	0.0126784426	0.0126784426	262.8378761841	262.8378762387
548	0.0126784426	0.0126784426	262.8378704249	262.8378762387
774	0.0126784426	0.0126784426	262.8378733743	262.8378762387
1094	0.0126784426	0.0126784426	262.8378748681	262.8378762387
1547	0.0126784426	0.0126784426	262.8378747120	262.8378762387
2187	0.0126784426	0.0126784426	262.8378735895	262.8378762386
3092	0.0126784426	0.0126784426	262.8378735598	262.8378762387
4372	0.0126784426	0.0126784426	262.8378738956	262.8378762387
6182	0.0126784426	0.0126784426	262.8378734302	262.8378762387

[a] $\zeta_\perp = 250$; $\zeta_z = 1.8$. [b] $Re\{\zeta_\perp \overline{P'C_{1\perp}}^2\} = 0$; $Im\{\zeta_\perp \overline{P'C_{1\perp}}^2\} = 0$; $\zeta_z \overline{P'C_{1z}}^2 = 0$. [c] $Re\{\zeta_\perp \overline{P'C_{2\perp}}^2\} = -15$; $Im\{\zeta_\perp \overline{P'C_{2\perp}}^2\} = 20$; $\zeta_z \overline{P'C_{2z}}^2 = 0$.

The following integrals are analogous to the higher-order incomplete gamma functions:

$$I(\hat{\xi}, \overrightarrow{P''Q''})^{(\vec{n})} \equiv \int_0^1 \frac{dt}{\zeta_z t^2 + \zeta_\perp (1-t^2)} \times \left\{ \frac{\zeta_z t^2}{\zeta_z t^2 + \zeta_\perp (1-t^2)} \right\}^{n_x+n_y} t^{2n_z} \times \exp\left\{ -\overline{P''Q''}_\perp{}^2 \zeta_\perp \frac{\zeta_z t^2}{\zeta_z t^2 + \zeta_\perp (1-t^2)} - \overline{P''Q''}_z{}^2 \zeta_z t^2 \right\} \quad \text{(A22)}$$

The vertical recurrence relation is given by the following equation:[76]

$$((\vec{a}+\vec{1}_x)_A * \vec{0}_B r_{12}{}^{-1} \vec{0}_C * \vec{0}_D)^{(\vec{n})} = \left[\prod_{i=x,y,z} \left(\frac{\partial}{\partial J_{i,1}} - A_i \right)^{a_i} \times \left(\frac{\partial}{\partial J_{x,1}} - A_x \right) (\vec{0}_A * \vec{0}_B r_{12}{}^{-1} \vec{0}_C * \vec{0}_D)_{\vec{J}1,\vec{J}2}{}^{(\vec{n})} \right]_{\vec{J}1=J2=0}$$

$$= \overline{P'A}_x (\vec{a}_A * \vec{0}_B r_{12}{}^{-1} \vec{0}_C * \vec{0}_D)^{(\vec{n})} - \frac{\rho_x}{\zeta_{ab,x}} \overline{P'Q'}_x \times (\vec{a}_A * \vec{0}_B r_{12}{}^{-1} \vec{0}_C * \vec{0}_D)^{(\vec{n}+\vec{1}_x)} - \left(\frac{1}{2}\right) a_x \zeta_{ab,x}{}^{-1} \left\{ ((\vec{a}-\vec{1}_x)_A * \vec{0}_B r_{12}{}^{-1} \vec{0}_C * \vec{0}_D)^{(\vec{n})} - \frac{\rho_x}{\zeta_{ab,x}} ((\vec{a}-\vec{1}_x)_A * \vec{0}_B r_{12}{}^{-1} \vec{0}_C * \vec{0}_D)^{(\vec{n}+\vec{1}_x)} \right\} \quad \text{(A23)}$$

In the aforementioned calculation, initially, the inner differentiation was executed, then $\overline{P''A}_x$ and $\overline{P''Q''}_x$ were exchanged with the differential operators, $\prod_{i=x,y,z} (\partial/\partial J_{i,1} - A_i)^{a_i}$. The important modifications of eq A23 from the corresponding equation in ref 73 are that the vector $\vec{P}$ and the exponent $\zeta_{ab,\text{iso}}$ are replaced by the complex vector $\vec{P}'$ and $\zeta_{ab,x}$, respectively. The complex vector $\vec{P}'$ is given by the following equation:

$$\vec{P}' = \hat{\xi}_{ab}{}^{-1} (\hat{\xi}_a \vec{A} + \hat{\xi}_b \vec{B}) + \frac{i}{2} \hat{\xi}_{ab}{}^{-1} \vec{A}_{AB} \quad \text{(A24)}$$

In the same way, the LRL−HS recurrence relation[77,78] can be derived:

$$(\vec{a}_A * \vec{0}_B r_{12}{}^{-1} (\vec{c}+\vec{1}_x)_C * \vec{0}_D)^{(\vec{n})} = -\frac{\zeta_{ab,x}}{\zeta_{cd,x}} ((\vec{a}+\vec{1}_x)_A * \vec{0}_B r_{12}{}^{-1} \vec{c}_C * \vec{0}_D)^{(\vec{n})} + \left(\overline{Q'C}_x + \frac{\zeta_{ab,x}}{\zeta_{cd,x}} \overline{P'A}_x \right) (\vec{a}_A * \vec{0}_B r_{12}{}^{-1} \vec{c}_C * \vec{0}_D)^{(\vec{n})} + \left(\frac{1}{2}\right) c_x \zeta_{cd,x}{}^{-1} (\vec{a}_A * \vec{0}_B r_{12}{}^{-1} (\vec{c}-\vec{1}_x)_C * \vec{0}_D)^{(\vec{n})} + \left(\frac{1}{2}\right) a_x \zeta_{cd,x}{}^{-1} ((\vec{a}-\vec{1}_x)_A * \vec{0}_B r_{12}{}^{-1} \vec{c}_C * \vec{0}_D)^{(\vec{n})} \quad \text{(A25)}$$

The horizontal recurrence relation is simply derived from the following equation:[76]

$$\left(\frac{\partial}{\partial J_k} - B_k \right) = \left(\frac{\partial}{\partial J_k} - A_k \right) + \overline{AB}_k \quad \text{(A26a)}$$

$$(\vec{a}_A * (\vec{b}+\vec{1}_x)_B r_{12}{}^{-1} \vec{c}_C * \vec{d}_D)^{(\vec{n})} = ((\vec{a}+\vec{1}_x)_A * \vec{b}_B r_{12}{}^{-1} \vec{c}_C * \vec{d}_D)^{(\vec{n})} + \overline{AB}_x (\vec{a}_A * \vec{b}_B r_{12}{}^{-1} \vec{c}_C * \vec{d}_D)^{(\vec{n})} \quad \text{(A26b)}$$

The same relation is also satisfied for $\vec{c}$ and $\vec{d}$. Similar recurrence relations can be easily derived for the overlap and the electron-nucleus attraction integrals.

Appendix A-3. The Kinetic Integrals

The kinetic energy integrals are easily obtained from the overlap integrals. The operator of kinetic energy is defined by the following equation:

$$\hat{T} = \left(\frac{1}{2}\right) \vec{\Pi}^2 = \frac{1}{2} (-i\vec{\nabla} + \vec{A})^2 \quad \text{(A27)}$$

where $\vec{A}(\vec{r}) = {}^1/_2 \vec{B}_0 \times \vec{r}$ is the vector potential at $\vec{r}$ for the

symmetric gauge. The kinetic energy integrals are calculated from the overlap integrals:

$$(\vec{a}_{\mathrm{A}}^{*}\{\hat{T}\vec{b}_{\mathrm{B}}\}) = \frac{1}{2}\sum_{k=x,y,z}(\{\Pi_k\vec{a}_{\mathrm{A}}\}^{*}\{\Pi_k\vec{b}_{\mathrm{B}}\}) = \sum_{k=x,y,z}\left\{\left(\frac{1}{2}\right)a_k b_k((\vec{a}-\vec{1}_k)_{\mathrm{A}}^{*}(\vec{b}-\vec{1}_k)_{\mathrm{B}}) + 2\zeta_{a,k}\zeta_{b,k}((\vec{a}+\vec{1}_k)_{\mathrm{A}}^{*}(\vec{b}+\vec{1}_k)_{\mathrm{B}}) - a_k\zeta_{b,k}((\vec{a}-\vec{1}_k)_{\mathrm{A}}^{*}(\vec{b}+\vec{1}_k)_{\mathrm{B}}) - b_k\zeta_{a,k}((\vec{a}+\vec{1}_k)_{\mathrm{A}}^{*}(\vec{b}-\vec{1}_k)_{\mathrm{B}})\right\} + \left(\frac{1}{8}\right)B_0{}^2\sum_{l=x,y}((\vec{a}+\vec{1}_l)_{\mathrm{A}}^{*}(\vec{b}+\vec{1}_l)_{\mathrm{B}}) + \left(\frac{1}{4}\right)iB_0\{a_y((\vec{a}-\vec{1}_y)_{\mathrm{A}}^{*}(\vec{b}+\vec{1}_x)_{\mathrm{B}}) - a_x((\vec{a}-\vec{1}_x)_{\mathrm{A}}^{*}(\vec{b}+\vec{1}_y)_{\mathrm{B}}) - b_y((\vec{a}+\vec{1}_x)_{\mathrm{A}}^{*}(\vec{b}-\vec{1}_y)_{\mathrm{B}}) + b_x((\vec{a}+\vec{1}_y)_{\mathrm{A}}^{*}(\vec{b}-\vec{1}_x)_{\mathrm{B}}) + 2(\zeta_{a,x}+\zeta_{b,y})((\vec{a}+\vec{1}_x)_{\mathrm{A}}^{*}(\vec{b}+\vec{1}_y)_{\mathrm{B}}) - 2(\zeta_{a,y}+\zeta_{b,x})((\vec{a}+\vec{1}_y)_{\mathrm{A}}^{*}(\vec{b}+\vec{1}_x)_{\mathrm{B}})\} \quad \text{(A28)}$$

To use the aforementioned formula, the overlap matrices $((\vec{a}+\vec{1}_k)_{\mathrm{A}}^{*}(\vec{b}+\vec{1}_l)_{\mathrm{B}})$ were calculated.

Appendix A-4. The Numerical Integration of Coulomb Integrals

If the exponents are very anisotropic ($\zeta_\perp \gg \zeta_z$), the term $\{1 - t^2(\zeta_\perp - \zeta_z)/\zeta_\perp\}^{-1}$ in eq A22 almost diverges at $t \approx 1$. The ordinary numerical integrations, such as the Gauss−Legendre quadrature, were inefficient. This difficulty was resolved by the double exponential transformation:[59]

$$t = \tanh\left(\frac{\pi}{2}\sinh\upsilon\right) \quad \text{(A29)}$$

The new variable (υ) was sampled at the evenly distributed points in the range from 0 to π. In Table A1, we compare the convergence of the two integration procedures: the Gauss−Legendre method (GL) and the double-exponential formular (DE). The DE formula shows rapid convergence. In this paper, the number of sampling points was 100 or 1000.

Acknowledgment. We thank Dr. Robin Challoner for correcting the manuscript.

References and Notes

(1) Abrikosov, A. A. *Fundamentals of the Theory of Metals*; North−Holland: Amsterdam, 1988.
(2) Aschcroft, N. W.; Mermin, N. D. *Solid State Physics*; Holt, Rinehart, and Winston: New York, 1976.
(3) London, F. *Superfluids, Macroscopic Theory of Superconductivity*; Wiley: New York, 1950.
(4) Byers, N.; Yang, C. N. *Phys. Rev. Lett.* **1961**, *7*, 46−49.
(5) Cheung, H.-F.; Gefen, Y.; Riedel, E. K.; Shih, W.-H. *Phys. Rev. B* **1988**, *37*, 6050−6062.
(6) Deaver, B. S., Jr.; Fairbank, W. M. *Phys. Rev. Lett.* **1961**, *7*, 43−46.
(7) Doll, R.; Naebauer, M. *Phys. Rev. Lett.* **1961**, *7*, 51−52.
(8) Little, W. A.; Parks, R. D. *Phys. Rev. Lett.* **1962**, *9*, 9−12.
(9) Imry, Y. *Introduction to Mesoscopic Physics*; Oxford University Press: New York, 1997.
(10) Warburton, R. J.; Schaflein, C.; Haft, D.; Bickel, F.; Lorke, A.; Karrai, K.; Garcia, J. M.; Schoenfeld, W.; Petroff, P. M. *Nature* **2000**, *405*, 926−929.
(11) Bayer, M.; Korkusinski, M.; Hawrylak, P.; Gutbrod, T.; Michel, M.; Forchel, A. *Phys. Rev. Lett.* **2003**, *90*, 186801-1−186801-4.
(12) Ajiki, H.; Ando, T. *J. Phys. Soc. Jpn.* **1993**, *62*, 1255−1266.
(13) Saito, R.; Dresselhaus, G.; Dresselhaus, M. S. *Physical Properties of Carbon Nanotubes*; Imperial College Press: London, 1998.
(14) Bachtold, A.; Strunk, C.; Salvetat, J.-P.; Bonard, J.-M.; Forro, L.; Nussbaumer, T.; Schonenberger, C. *Nature* **1999**, *397*, 673−675.
(15) Minot, E. D.; Yaish, Y.; Sazonova, V.; McEuen, P. L. *Nature* **2004**, *428*, 536−539.
(16) Cao, J.; Wang, Q.; Rolandi, M.; Dai, H. *Phys. Rev. Lett.* **2004**, *93*, 216803-1−216803-4.
(17) Zaric, S.; Ostojic, G. N.; Kono, J.; Shaver, J.; Moore, V. C.; Strano, M. S.; Hauge, R. H.; Smalley, R. E.; Wei, X. *Science* **2004**, *304*, 1129−1131.
(18) London, F. *J. Chem. Phys.* **1937**, *5*, 837−838.
(19) Kubo, A. *Abstr. Pap. Am. Chem. Soc.* **2003**, *226*, U326.
(20) Soncini, A.; Fowler, P. W. *Chem. Phys. Lett.* **2004**, *400*, 213−220.
(21) Schiff, L. I.; Snyder, H. *Phys. Rev.* **1939**, *55*, 0059−0063.
(22) Elliott, R. J.; Loudon, R. *J. Phys. Chem. Solids* **1960**, *15*, 196−207.
(23) Cohen, R.; Lodenqua, J.; Ruderman, M. *Phys. Rev. Lett.* **1970**, *25*, 467.
(24) Rosner, W.; Wunner, G.; Herold, H.; Ruder, H. *J. Phys. B* **1984**, *17*, 29−52.
(25) Bouferguene, A.; Weatherford, C. A.; Jones, H. W. *Phys. Rev. E* **1999**, *59*, 2412−2423.
(26) Kravchenko, Y. P.; Liberman, M. A.; Johansson, B. *Phys. Rev. Lett.* **1996**, *77*, 619−622.
(27) Kravchenko, Y. P.; Liberman, M. A.; Johansson, B. *Phys. Rev. A* **1996**, *54*, 287−305.
(28) Kravchenko, Y. P.; Liberman, M. A. *Int. J. Quantum Chem.* **1997**, *62*, 593−601.
(29) Garstang, R. H. *Rep. Prog. Phys.* **1977**, *40*, 105−154.
(30) Lai, D. *Rev. Mod. Phys.* **2001**, *73*, 629−661.
(31) Ruder, H.; Herold, H.; Geyer, F.; Wunner, G. *Atoms in Strong Magnetic Fields: Quantum Mechanical Treatment and Applications in Astrophysics and Quantum Chaos*; Springer−Verlag: Berlin, 1994.
(32) Schmelcher, P.; Schweizer, W. *Atoms and Molecules in Strong External Fields*; Plenum Press: New York, 1998.
(33) Runge, K.; Sabin, J. R. *Int. J. Quantum Chem.* **1997**, *64*, 495−496.
(34) Boys, S. F. *Proc. R. Soc. London, A* **1950**, *200*, 542−554.
(35) Huzinaga, S. *J. Chem. Phys.* **1965**, *42*, 1293−1302.
(36) Schaefer, H. F. *Quantum Chemistry*; Clarendon Press: Oxford, U.K., 1984.
(37) Davidson, E. R.; Feller, D. *Chem. Rev.* **1986**, *86*, 681−696.
(38) Larsen, D. M. *Phys. Rev. A* **1982**, *25*, 1295−1304.
(39) Wille, U. *Phys. Rev. A* **1988**, *38*, 3210−3235.
(40) Zaucer, M.; Azman, A. *Phys. Rev. A* **1978**, *18*, 1320−1321.
(41) Ortiz, G.; Jones, M. D.; Ceperley, D. M. *Phys. Rev. A* **1995**, R3408.
(42) Liberman, M. A.; Petrov, A. V. *Phys. Scr.* **1998**, *57*, 573−580.
(43) Kravchenko, Y. P.; Liberman, M. A. *Phys. Rev. A* **1998**, *57*, 3403−3418.
(44) Neuhauser, D.; Koonin, S. E.; Langanke, K. *Phys. Rev. A* **1987**, *36*, 4163−4175.
(45) Lai, D.; Salpeter, E. E.; Shapiro, S. L. *Phys. Rev. A* **1992**, *45*, 4832−4847.
(46) Demeur, M.; Heenen, P. H.; Godefroid, M. *Phys. Rev. A* **1994**, *49*, 176−183.
(47) Schmelcher, P.; Cederbaum, L. S. *Phys. Rev. A* **1988**, *37*, 672−681.
(48) London, F. *J. Phys. Radium* **1937**, *8*, 397−409.
(49) Pople, J. A. *J. Chem. Phys.* **1962**, *37*, 53−59.
(50) Kappes, U.; Schmelcher, P. *J. Chem. Phys.* **1994**, *100*, 2878−2887.
(51) Kappes, U.; Schmelcher, P. *Phys. Rev. A* **1995**, *51*, 4552−4557.
(52) Kappes, U.; Schmelcher, P. *Phys. Lett. A* **1996**, *210*, 409−415.
(53) Kappes, U.; Schmelcher, P. *Phys. Rev. A* **1996**, *53*, 3869−3883.
(54) Kappes, U.; Schmelcher, P. *Phys. Rev. A* **1996**, *54*, 1313−1317.
(55) Detmer, T.; Schmelcher, P.; Diakonos, F. K.; Cederbaum, L. S. *Phys. Rev. A* **1997**, *56*, 1825−1838.
(56) Detmer, T.; Schmelcher, P.; Cederbaum, L. S. *Phys. Rev. A* **1998**, *57*, 1767−1777.
(57) Kravchenko, Y. P.; Liberman, M. A. *Int. J. Quantum Chem.* **1997**, *64*, 513−522.
(58) Jones, M. D.; Ortiz, G.; Ceperley, D. M. *Phys. Rev. A* **1999**, *59*, 2875−2885.
(59) Takahashi, H.; Mori, M. *Publ. RIMS, Kyoto Univ.* **1974**, *9*, 721−741.
(60) Turbiner, A. V. *J. Phys. A* **1984**, *17*, 859−875.
(61) Gallas, J. A. C. *J. Phys. B* **1985**, *18*, 2199−2206.
(62) Rech, P. C.; Gallas, M. R.; Gallas, J. A. *J. Phys. B* **1986**, *19*, L215−L219.
(63) Chen, Z. H.; Goldman, S. P. *Phys. Rev. A* **1992**, *45*, 1722−1731.
(64) Vincke, M.; Baye, D. *J. Phys. B* **1985**, *18*, 167−176.
(65) Shavitt, I.; Karplus, M. *J. Chem. Phys.* **1962**, *36*, 550−551.
(66) Schmidt, M. W.; Ruedenberg, K. *J. Chem. Phys.* **1979**, *71*, 3951−3962.
(67) Feller, D. F.; Ruedenberg, K. *Theor. Chim. Acta* **1979**, *52*, 231−251.

(68) Mclean, A. D.; Weiss, A.; Yoshimine, M. *Rev. Mod. Phys.* **1960**, *32*, 211−218.
(69) Krishnan, R.; Binkley, J. S.; Seeger, R.; Pople, J. A. *J. Chem. Phys.* **1980**, *72*, 650−654.
(70) Boys, S. F. *Proc. R. Soc. London, A* **1960**, *258*, 402−411.
(71) Rys, J.; Dupuis, M.; King, H. F. *J. Comput. Chem.* **1983**, *4*, 154−157.
(72) Mcmurchie, L. E.; Davidson, E. R. *J. Comput. Phys.* **1978**, *26*, 218−231.
(73) Obara, S.; Saika, A. *J. Chem. Phys.* **1986**, *84*, 3963−3974.
(74) Ishida, K. *J. Chem. Phys.* **2003**, *118*, 4819−4831.
(75) Singer, K. *Proc. R. Soc. London, A* **1960**, *258*, 412−420.
(76) Head-Gordon, M.; Pople, J. A. *J. Chem. Phys.* **1988**, *89*, 5777−5786.
(77) Lindh, R.; Ryu, U.; Liu, B. *J. Chem. Phys.* **1991**, *95*, 5889−5897.
(78) Hamilton, T. P.; Schaefer, H. F. *Chem. Phys.* **1991**, *150*, 163−171.